GEOPHYSICS, VOL. 68, NO. 6 (NOVEMBER-DECEMBER 2003); P. 1952–1961, 6 FIGS., 2 TABLES.
10.1190/1.1635049

A combined analytic signal and Euler method (AN-EUL) for automatic interpretation of magnetic data

Ahmed Salem* and Dhananjay Ravat‡

ABSTRACT

We present a new automatic method of interpretation of magnetic data, called AN-EUL (pronounced "an oil"). The derivation is based on a combination of the analytic signal and the Euler deconvolution methods. With AN-EUL, both the location and the approximate geometry of a magnetic source can be deduced. The method is tested using theoretical simulations with different magnetic models placed at different depths with respect to the observation height. In all cases, the method estimated the locations and the approximate geometries of the sources. The method is tested further using ground magnetic data acquired above a shallow geological dike whose source parameters are known from drill logs, and also from airborne magnetic data measured over a known ferrometallic object. In both these cases, the method correctly estimated the locations and the nature of these sources.

INTRODUCTION

A variety of semiautomatic methods, based on the use of derivatives of the magnetic anomalies, have been developed for the determination of causative source parameters such as locations of boundaries and depths. One of these techniques is the method of the analytic signal for magnetic anomalies, which was initially used in its complex function form and makes use of the properties of the Hilbert transform (Nabighian, 1972; Atchuta Rao et al., 1981; Nelson, 1988; Pedersen, 1989; Roest et al., 1992). Initially, it was successfully applied on profile data to locate dikelike bodies (Nabighian, 1972, 1974, 1984; Atchuta Rao et al., 1981). The method was further developed by Roest et al. (1992) for the interpretation of aeromagnetic maps (see also MacLeod et al., 1993). Moreover, Bastani and Pedersen (2001) employed the method to estimate many parameters of dikelike bodies, including depth, strike, dip, width, and magnetization. Also, Salem et al. (2002) demonstrated the feasibility of the method to locate compact magnetic objects often encountered in environmental applications.

The success of the analytic signal method results from the fact that source locations of magnetic anomalies are obtained using only a few assumptions. For example, horizontal positions are estimated by the maxima of the amplitude of the analytic signal (*AAS*). In addition, depths can be obtained from the shape of the *AAS* (Roest et al., 1992) or based on the ratio of the *AAS* to its higher derivatives (Hsu et al., 1996, 1998; Bastani and Pedersen, 2001; Salem et al., 2002). However, a correct estimate of the depth is obtained only when the source corresponds to the chosen model (Thurston and Smith, 1997). Several attempts have been made to enable the analytic signal method to estimate both the depth and model type of magnetic sources (e.g., Debeglia and Corpel, 1997; Smith et al., 1998; Hsu et al., 1998; Thurston et al., 1999).

In this paper, we present a new method that circumvents some of the limitations of previous studies and determines the location coordinates as well as source geometry from the observed anomaly. The method is derived by substituting an appropriate derivative of Euler's equation into the expression of the analytic signal of the magnetic field and, hence, we call it AN-EUL (pronounced "an oil"). With AN-EUL, both the depth and the nature of a magnetic source are simultaneously determined at the location of maxima of the *AAS* function. We have generalized the method for both 2D and 3D applications (i.e., profiles as well as gridded magnetic anomaly data). The utility of the method is demonstrated using theoretical and field examples from geological and environmental applications.

THE AN-EUL METHOD

Since our method is based on substituting derivatives of Euler's equation into the analytic signal equation to estimate simultaneously the source parameters generally sought from

Manuscript received by the Editor August 24, 2001; revised manuscript received May 30, 2003.
*Kyushu University, Earth Resources Engineering Department, Hakozaki 6-10-1, Fukuoka 812-8581, Japan; and Nuclear Materials Authority of Egypt, Airborne Geophysics Department, Kattamiya Road, Maddi, P.O. Box 530, Cairo, Egypt. E-mail: ahmedsalem30@hotmail.com.
‡Southern Illinois University at Carbondale, Department of Geology MS 4234, Carbondale, Illinois 62901-4342. E-mail: ravat@geo.siu.edu.

the Euler method, we briefly describe the necessary aspects of these methods first.

The analytic signal method

The complex analytic signal (Nabighian, 1972) can be defined in terms of the total field T and its Hilbert transform or in terms of the horizontal and vertical derivatives of the total field T. The latter definition is

$$A(x,y) = \left(\frac{\partial T}{\partial x}\hat{x} + \frac{\partial T}{\partial y}\hat{y} + i\frac{\partial T}{\partial z}\hat{z}\right), \quad (1)$$

where $\hat{x}$, $\hat{y}$, $\hat{z}$ are unit vectors in the x, y, and z directions, i is the imaginary number $\sqrt{-1}$, $\partial T/\partial z$ is the vertical and $\partial T/\partial x$ and $\partial T/\partial y$ are the horizontal derivatives of the magnetic field. The 3D expression of the AAS is given by Roest et al. (1992) as

$$|AAS(x,y)| = \sqrt{\left(\frac{\partial T}{\partial x}\right)^2 + \left(\frac{\partial T}{\partial y}\right)^2 + \left(\frac{\partial T}{\partial z}\right)^2}. \quad (2)$$

The amplitude of the nth-order derivative analytic signal can be expressed (Debeglia and Corpel, 1997) as

$$|AAS_n(x,y)| = \sqrt{\left(\frac{\partial T_n^z}{\partial x}\right)^2 + \left(\frac{\partial T_n^z}{\partial y}\right)^2 + \left(\frac{\partial T_n^z}{\partial z}\right)^2}, \quad (3)$$

where superscript z denotes the vertical derivative of the field. The AAS and its higher order derivatives can be easily computed in a number of ways. The horizontal derivatives can be calculated directly from a total field grid using a simple 3×3 difference filter. Also, both the horizontal and vertical gradients can be calculated in the frequency domain using conventional fast Fourier transform (FFT) techniques (Blakely, 1995).

The Euler method

Potential fields satisfy Laplace's equation outside the source regions; the equation is homogeneous for specific source geometries (Blakely, 1995). A homogeneous equation also satisfies Euler's equation (Thompson, 1982; Blakely, 1995; Ravat, 1996a). The 3D form of Euler's equation can be defined (Reid et al., 1990) as

$$x\frac{\partial T}{\partial x} + y\frac{\partial T}{\partial y} + z\frac{\partial T}{\partial z} + \eta T = x_o\frac{\partial T}{\partial x} + y_o\frac{\partial T}{\partial y} + z_o\frac{\partial T}{\partial z} + \eta b, \quad (4)$$

where x, y, and z are the coordinates of a measuring point; x_o, y_o, and z_o are the coordinates of the source location; b is a base level; and η is a structural index defining the anomaly attenuation rate at the observation location [e.g., $\eta = 0$ for a contact, $\eta = 1$ for the top of a vertical dike or the edge of a sill, $\eta = 2$ for the center of a horizontal or vertical cylinder, and $\eta = 3$ for the center of a magnetic sphere or a dipole (Thompson, 1982; Reid et al., 1990)].

The AN-EUL derivation

Taking the derivatives of Euler's equation (4) in the x, y, and z directions and setting $x = x_o$, $y = y_o$, and $z = 0$ (i.e., taking the observation point above the center of the source, which we term the epi-centroid), we get

$$z_o\left(\frac{\partial^2 T}{\partial z \partial x}\right)_{x=x_o,y=y_o} = (\eta+1)\left(\frac{\partial T}{\partial x}\right)_{x=x_o,y=y_o}, \quad (5a)$$

$$z_o\left(\frac{\partial^2 T}{\partial z \partial y}\right)_{x=x_o,y=y_o} = (\eta+1)\left(\frac{\partial T}{\partial y}\right)_{x=x_o,y=y_o}, \quad (5b)$$

$$z_o\left(\frac{\partial^2 T}{\partial z^2}\right)_{x=x_o,y=y_o} = (\eta+1)\left(\frac{\partial T}{\partial z}\right)_{x=x_o,y=y_o}. \quad (5c)$$

Squaring equations (5a), (5b), and (5c), summing, and taking the square root, we obtain

$$z_o\left(\sqrt{\left(\frac{\partial^2 T}{\partial z \partial x}\right)^2 + \left(\frac{\partial^2 T}{\partial z \partial y}\right)^2 + \left(\frac{\partial^2 T}{\partial z^2}\right)^2}\right)_{x=x_o,y=y_o} = (\eta+1)\left(\sqrt{\left(\frac{\partial T}{\partial x}\right)^2 + \left(\frac{\partial T}{\partial y}\right)^2 + \left(\frac{\partial T}{\partial z}\right)^2}\right)_{x=x_o,y=y_o}. \quad (6a)$$

Equation (6a) can be expressed concisely as

$$z_o|AAS_1|_{x=x_o,y=y_o} = (\eta+1)|AAS_0|_{x=x_o,y=y_o}, \quad (6b)$$

where $|AAS_0|$ and $|AAS_1|$ are the amplitudes of the analytic signal of the anomaly and its first-order derivative, respectively. Equation (6b) implies that the depth of a magnetic source can be estimated based on the ratio of the AAS_0 and AAS_1 at the epi-centroid such that for a contact ($\eta = 0$),

$$z_o = \left|\frac{AAS_0}{AAS_1}\right|_{x=x_o,y=y_o}; \quad (7a)$$

thin dike ($\eta = 1$),

$$z_o = 2\left|\frac{AAS_0}{AAS_1}\right|_{x=x_o,y=y_o}; \quad (7b)$$

vertical or horizontal cylinder ($\eta = 2$),

$$z_o = 3\left|\frac{AAS_0}{AAS_1}\right|_{x=x_o,y=y_o}; \text{ and} \quad (7c)$$

dipole or sphere ($\eta = 3$),

$$z_o = 4\left|\frac{AAS_0}{AAS_1}\right|_{x=x_o,y=y_o}. \quad (7d)$$

Thus, the derivatives of Euler's equation enables generalized analytic signal formulas to estimate the depth of magnetic sources if the source type is known. Some of these equations have already been proven using other derivations [e.g., dipole model (Salem et al., 2002)] or the analytic signal [e.g., dike model (Bastani and Pedersen, 2001)]. The advantage of substituting Euler's equation into the expression of the AAS, however, is that generalized relations to estimate both the depth and model type can be found at the epi-centroid (generalized because many sources can be analyzed with the same operation of the entire function). An important advantage of the resulting AN-EUL method is that one is not restricted to idealized

sources (having fixed and integer η), but one can also work with changing, fractional η associated with arbitrarily-shaped sources (Ravat, 1996a).

To achieve the final step, taking the derivatives in the x, y, and z directions of the first vertical derivative of equation (4), then squaring, summing, and taking the square root as before, we obtain

$$z_o|AAS_2|_{x=x_o,y=y_o} = (\eta+2)|AAS_1|_{x=x_o,y=y_o}, \qquad (8)$$

where $|AAS_2|$ is the AAS of the second-order derivative of the anomaly. Substituting equation (8) in equation (6b), we obtain

$$\eta = \left(\frac{2|AAS_1|^2 - |AAS_2||AAS_0|}{|AAS_2||AAS_0| - |AAS_1|^2}\right)_{x=x_o,y=y_o} \qquad (9)$$

and

$$z_o = \left(\frac{|AAS_1||AAS_0|}{|AAS_2||AAS_0| - |AAS_1|^2}\right)_{x=x_o,y=y_o}. \qquad (10)$$

Equations (9) and (10) show that both the structural index (which indicates the geometry of the source) and depth of a magnetic anomaly can be simultaneously calculated from the

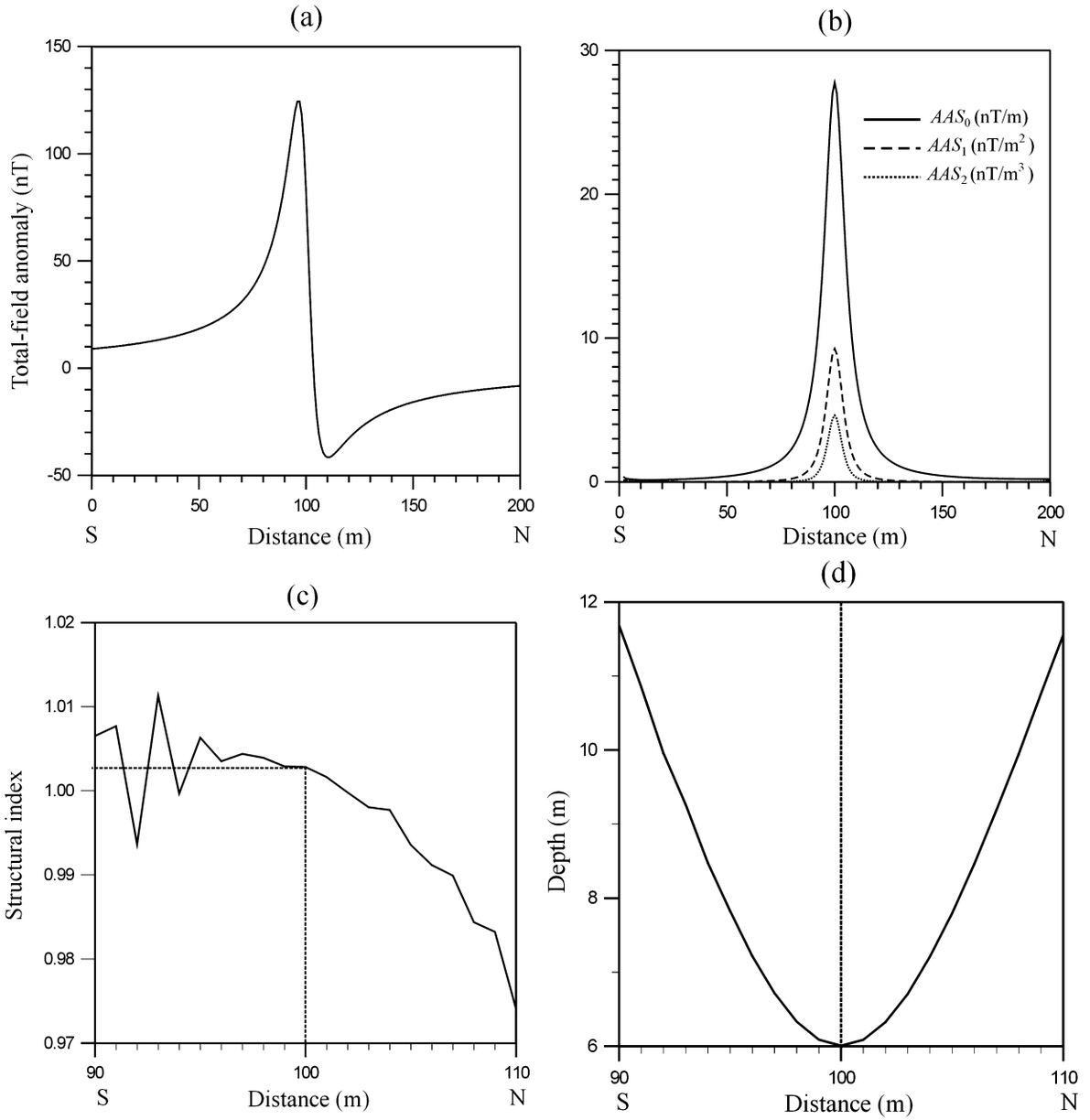

FIG. 1. (a) Total field magnetic anomaly for a thin vertical dike model located at $x = 100$ m and at the depth of 6 m, (b) analytic signal (AAS_0) and its first (AAS_1) and second (AAS_2) order derivatives, (c) estimated structural index (η) for the dike model at the epi-centroid location (100 m), and (d) estimated depth (z_o) for the dike model at the epi-centroid location (100 m).

AAS and its first-order and second-order derivatives at the epi-centroid. We can approximately estimate the epi-centroid itself based on the maximum of the *AAS*, and we have previously shown that inaccuracies due to such a determination are minimal (Salem et al., 2002).

THEORETICAL EXAMPLES

In this section, we test the AN-EUL method using synthetic magnetic data in both profile and grid form. We use magnetic anomaly data for an idealized model (thin dike) and a 3D model having magnetically nonidealized geometry (a steel drum). The appropriate derivatives of the magnetic anomalies for the synthetic models are calculated in the frequency domain using a conventional FFT technique.

The dike model

Figure 1a shows the total field magnetic anomaly of a thin vertical dike (with infinite depth extent) model. The anomaly values were calculated along a 200-m north-south profile at an interval of 1 m. The dike has a magnetization of 10 A/m and is located at the center of the profile. Its depth to the top is at 6 m with respect to observation locations. In this example, we used an induced field with a declination of 0° and an inclination of 60°. This source considers only induction; all the remaining sources in this paper have remanence. Both underlying methods have been demonstrated to work adequately with remanent magnetizations (Roest et al., 1992; Ravat, 1996a); none of the equations explicitly depend on magnetization characteristics, and thus are not affected by remanence.

Figure 1b shows curves of the AAS_0, AAS_1, and AAS_2 fields for the dike model. The estimate of the model type (structural index) and depth were calculated using equations (9) and (10) (Figures 1c and 1d). At the location of maximum AAS_0, the estimate of the depth (z_o) is 6.0 m and the model type (η) is nearly 1.0, indicating that the source parameters of the dike are accurately obtained using our method. However, as with all gradient interpretation methods, the resolution of our approach is a function of the data quality and noise. Generally, if noise is high wavenumber, its effect can be reduced by upward continuing the anomalies. Here, we present simulations of the results for the above theoretical anomaly by adding different sets of random noise, upward continuing the corrupted anomaly to several heights, and then estimating the source parameters for each case. We contaminated the above anomaly with five sets of random noise ranging from 2% to 10% of the calculated anomaly data at an interval of 2%. For each noise percentage, we applied upward continuation using different heights (from 1 m to 10 m at an interval of 1 m). Figures 2a and 2b show the estimate of the structural index and depth for each case. It is observed that, in the presence of noise, for small heights of upward continuation, the results are unstable and incorrect especially for the data contaminated with large percentages of noise. However, beyond a certain height (in our example, $\geq$4 m), the results are stable and accurate for all given percentages of noise. The convergence observed in the figures will break down as higher upward continuation levels will make the anomaly broader and smaller, and ultimately degrade the resolution for sources intended for analysis. Similarly, if a residual anomaly is not obtained a priori, then upward continuation may also cause neighboring anomalies to interfere with the anomaly of interest. Thus, the ideal level of upward continuation is the first continuation level producing consistent estimates and may be determined from plots similar to those shown in Figures 2a and 2b.

Upward continuation is also the remedy for dikes that cannot be considered thin. When the width of the dike is much greater than the depth to its top, the AAS_0 will be double-peaked (Hsu et al., 1998), showing the two edges of the dike. If the two peaks are well separated, then the edges can be regarded as geologic contacts ($\eta = 0$). Note that whether a dike can be regarded as "thick" or "thin" is dependent on the source-to-observation distance (see, for more details, Hsu et al., 1998). More importantly, in some situations, there is a transitional region where the AAS_0 will be single peaked, but AAS_1 and/or AAS_2 will be

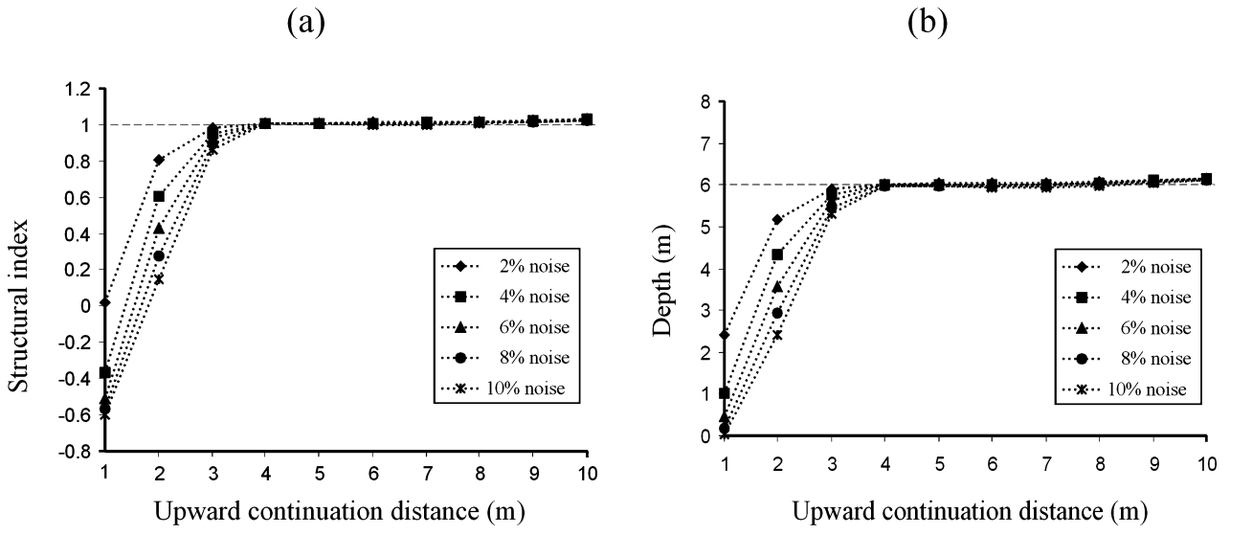

FIG. 2. Noise tests: (a) Estimate of the structural index (η) for the dike model (Figure 1a) after adding random noise and applying upward continuation, (b) estimate of the depth for the dike model (Figure 1a) after adding random noise and applying upward continuation.

double peaked. For the case of the observed dike later, which fell into the transitional region, we circumvent these difficulties by first upward continuing the anomalies to a point where all AAS_0, AAS_1, and AAS_2 are single-peaked.

The 3D arbitrarily-shaped model

Figure 3a shows the total field magnetic anomaly over a drum-shaped source used by Ravat (1996b). He had normalized observation spacing in terms of the survey heights measured in feet. Therefore, we present the results for this section in normalized distance units and give below both SI and non-SI units when appropriate. The drum (the model of his Drum #1) is vertical with a height of 0.9652 m (3.16 ft), external radius of 0.2921 m (0.95 ft), and thickness of 0.001 m. The inducing field intensity was 54000 nT with an inclination of 68° and the declination of 0°. The apparent susceptibility was 107.73 SI. The "apparent" remanent magnetization was 2739.3 A/m, with a remanent inclination of 61° and a remanent declination of 10°. The anomaly values are calculated using the code based on Talwani (1965) at an observation elevation of 1.524 m (5 ft) above the top of the drum and the spacing of 0.3048 m (1 ft). Figures 3b and 3c show curves of the amplitudes of the analytic signal and its first- and second-order derivatives (AAS_0, AAS_1, and AAS_2, respectively) along two profiles passing above the drum and oriented in the west-east and south-north directions.

Figures 3d and 3e show the estimate of the structural index along the two profiles using equation (9). At the epi-centroid,

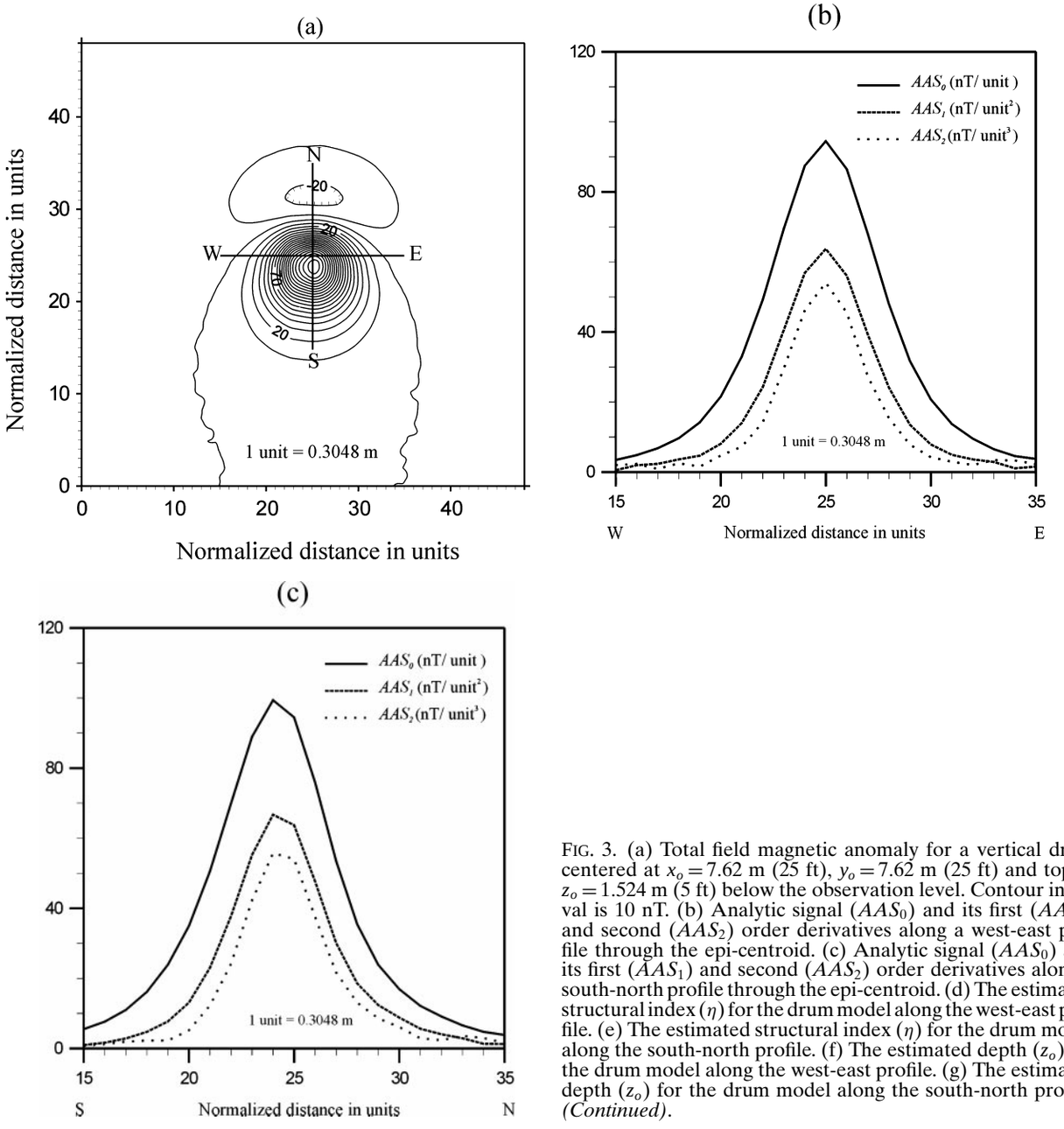

FIG. 3. (a) Total field magnetic anomaly for a vertical drum centered at $x_o = 7.62$ m (25 ft), $y_o = 7.62$ m (25 ft) and top at $z_o = 1.524$ m (5 ft) below the observation level. Contour interval is 10 nT. (b) Analytic signal (AAS_0) and its first (AAS_1) and second (AAS_2) order derivatives along a west-east profile through the epi-centroid. (c) Analytic signal (AAS_0) and its first (AAS_1) and second (AAS_2) order derivatives along a south-north profile through the epi-centroid. (d) The estimated structural index (η) for the drum model along the west-east profile. (e) The estimated structural index (η) for the drum model along the south-north profile. (f) The estimated depth (z_o) for the drum model along the west-east profile. (g) The estimated depth (z_o) for the drum model along the south-north profile. *(Continued)*.

η is 2.88, approaching the value of a dipole source ($\eta = 3$). The estimated depth (Figures 3f and 3g) at the epi-centroid using equation (10) is 1.75 m (5.76 ft), which falls within the dimension of the drum (with 0.25-m error from the center of the drum) and thus the level of error (12%) is acceptable for its intended application.

APPLICATION TO FIELD DATA

We present two examples from geological and environmental applications. Figure 4a shows total-field anomaly measured over an altered peridotitic dike in southern Illinois over a farm that has leased the underground mining rights to a coal company. The dike strikes in a northerly direction and the magnetic profile was obtained in the east-west direction at about 1.82 m observation elevation and with a spacing of about 7.62 m (Kirkham, 2001). From closely-spaced drilling done by the coal mining company, it is known that the depth to the top of the dike (from the surface) is about 10 m and its width is also about the same. The existence of a number of such dikes in this area is inferred from an analysis of the high-resolution aeromagnetic survey carried out by the U.S. Geological Survey (Hildenbrand and Ravat, 1997), and the coal company was interested in precisely locating these dikes without expensive drilling because the dikes obstruct their mining operations.

The ground magnetic data over the dike presented the transitional situation previously discussed (i.e., single-peaked AAS_0, but multipeaked AAS_1 and AAS_2 as a result of the

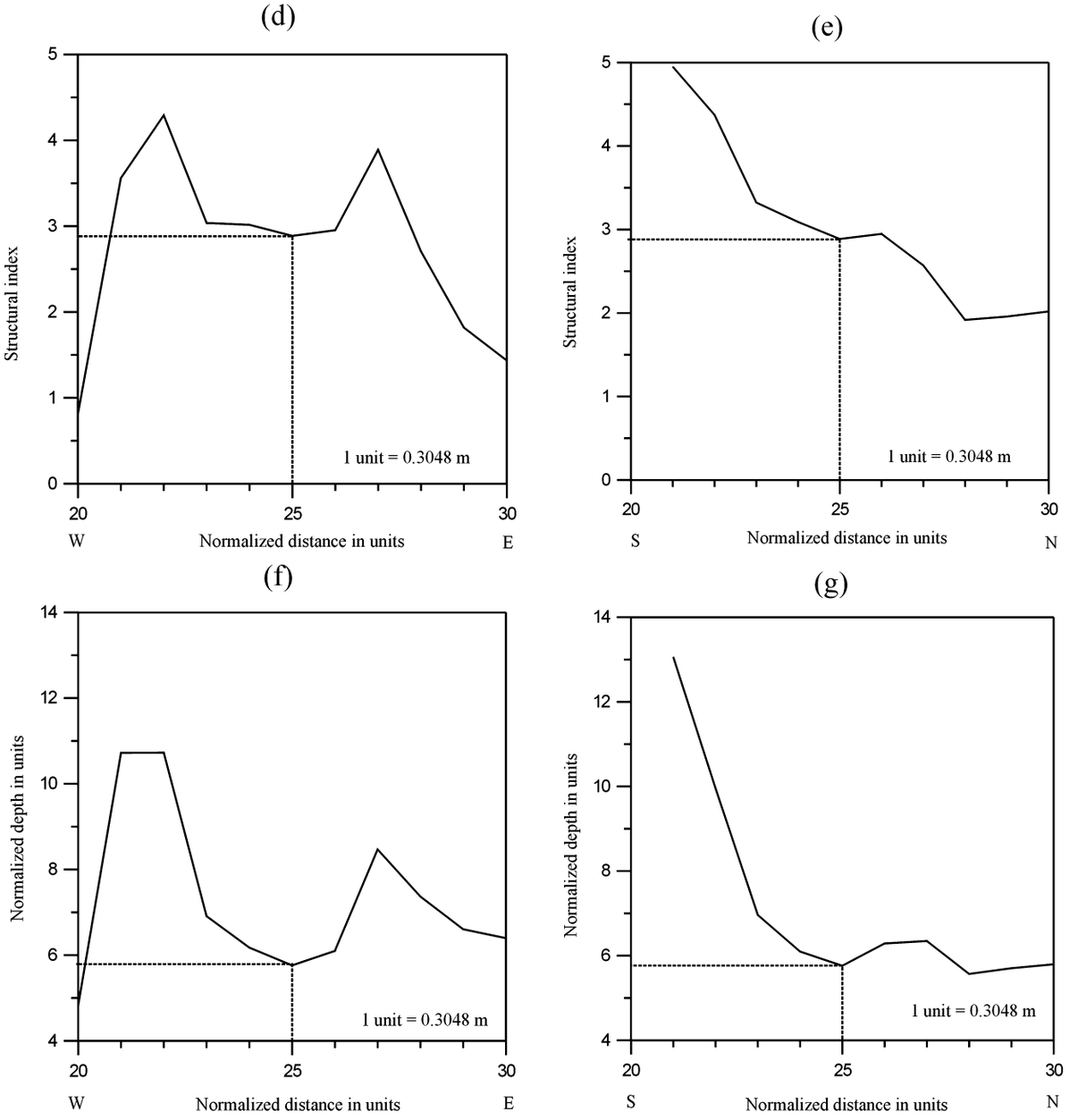

FIG. 3. *(Continued).*

width-to-depth ratio). The use of the profile was complicated further by measurement noise, inaccuracies due to coarse sampling (7.6 m) (the sampling was adequate for the original purpose, however), and also the actual geologic variation—a peridotitic dike is magnetic only because it is oxidized (based on Wasilewski and Mayhew, 1992, and references therein) and, in this near-surface environment, it is differentially oxidized [as substantiated by hand-examined samples and measured susceptibility variations (Kirkham, 2001)]. The ground magnetic data were transformed to the frequency domain using the FFT technique. The dike is relatively thick, but the upward-continuation distance of 10 m was adequate to achieve nearly single-peaked fields of the AAS_0, AAS_1, and AAS_2 with maxima located directly above the dike (Figures 4b–d). Table 1 shows the results of the AN-EUL method. The geometry of the source interpreted from the observed anomaly attenuation rate at the location of the maximum in AAS_0 is 1.27, indicating that even

Table 1. The AN-EUL results from the ground magnetic data over a dike in southern Illinois.

AAS_0 (nT/m)	AAS_1 (nT/m^2)	AAS_2 (nT/m^3)	η	z_o (m)
2.981	0.323	0.050	1.27	9.17*

*After subtracting the upward-continuation distance (10 m) and observation altitude (1.82 m).

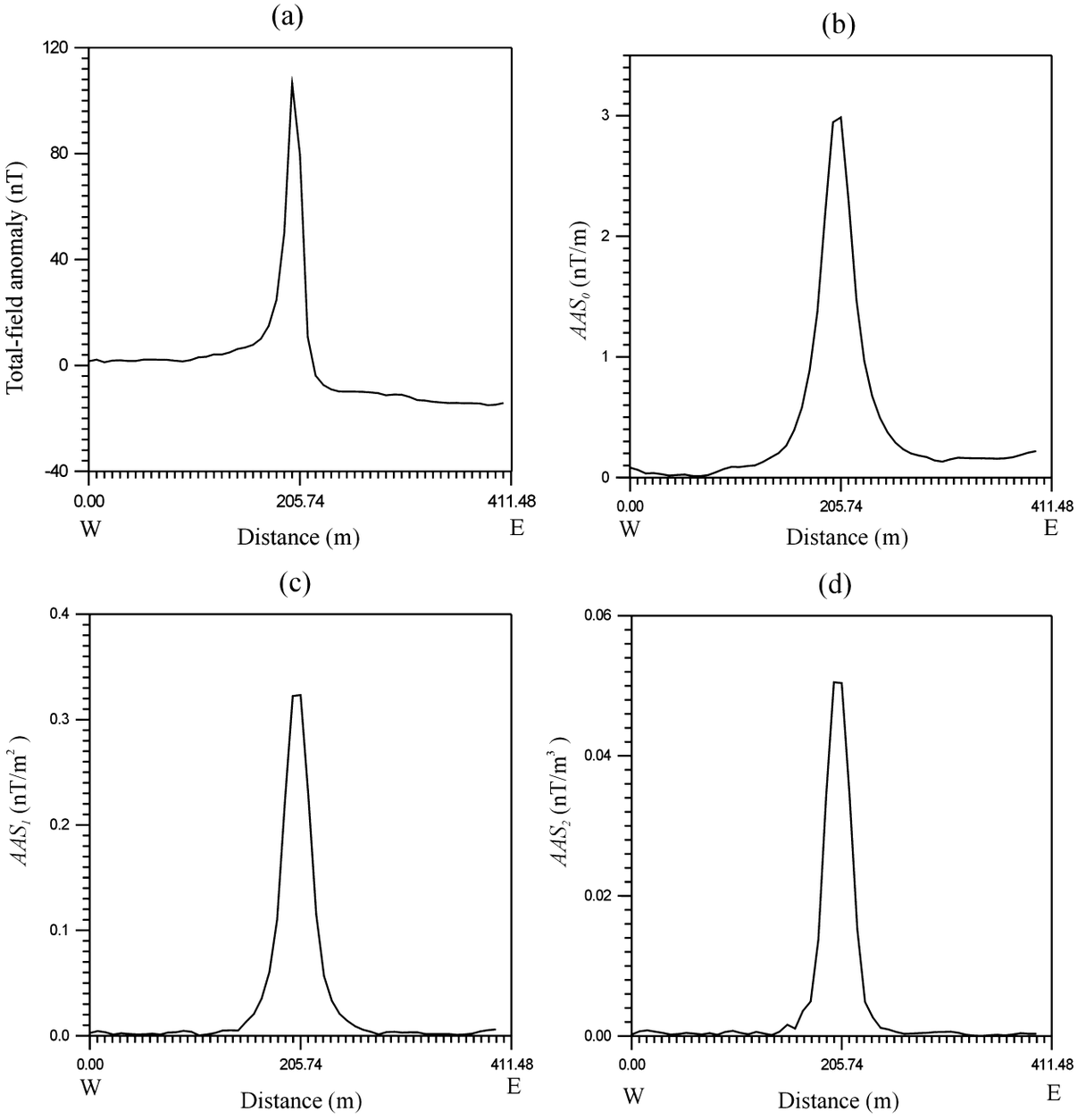

FIG. 4. (a) Total-field anomaly data from an igneous dike in southern Illinois (Kirkham, 2001), (b) analytic signal (AAS_0), (c) first-order derivative of the analytic signal (AAS_1), and (d) second-order derivative of the analytic signal (AAS_2).

from the upward-continued elevation the source appears to be a slightly thick dike (a misinterpretation that it could be the edge of a sill was avoided by examining the anomaly in profile and map forms). The estimated depth, after subtracting the upward-continuation height (10 m) and the observation elevation (1.82 m), is 9.17 m, which is consistent with the actual depth (about 10 m). With respect to the upward-continued anomaly elevation, the depth error (0.83 m) is less than 4% of the true source-to-observation distance (21.82 m).

To ensure the stability of our method, we perturbed the field data with 30 different sets of pseudorandom noise in the range of ± 2 nT. Then we applied the method using 30 different upward-continuation distances (from 11 m to 40 m at an interval of 1 m). Figures 5a shows estimates of the structural index, which indicate that the source is a dike. For all cases, the percent error in the estimated depths is less than 10% of the respective source-to-observation distances (Figure 5b). This exercise demonstrates the stability of the present method to estimate both the depth and model type.

The second example (Figure 6a) consists of an airborne magnetic anomaly over a ferrometallic object at the Badlands Bombing Range, South Dakota, test site measured using a Bell 206L-3 helicopter equipped with Geometrics G-822A cesium vapor optically pumped magnetometers with sensitivity of 0.001 nT [see Gamey et al. (2000) for the survey and the site description]. The object is an I-beam section with a mass of 13 kg, a length of 0.37 m, and a diameter of 0.11 m. This object is centered at $x = 8$ m, $y = 9$ m from the origin of the grid-based data of Figure 6a and buried horizontally in the east-west direction at a depth of 0.45 m from the surface. The survey was conducted on flight traverses directed approximately from north to south with a nominal spacing between traverses of 3 m. Aircraft ground speed was maintained at approximately 20 m/s, resulting in a sampling of approximately 0.4 m. The sensor altitude above the I-beam section was 1.67 m, giving a source-to-observation distance (to the center of the source) of 2.17 m.

The airborne magnetic data were interpolated at a spacing of 1 m and transformed to the frequency domain for the computation of the required quantities (Figures 6b–d). The maximum values of the AAS_0, AAS_1, and AAS_2 are located directly above the object. Table 2 lists the results of the η and the depth using the AN-EUL method. The nature of the source from the derived anomaly attenuation rate ($\eta = 2.47$) is reasonable for an arbitrarily-shaped object at a close distance, illustrating once again that the AN-EUL method is not restricted to idealized sources (having fixed and integer η), but it can also work with sources with fractional η which change with the source-to-observation distance. As in the Euler method, it is the η and the nature of the horizontal extension of the source (indicated from the anomaly profile or a map) that determines whether the depth mapping is done to the top of the source or the center (e.g., tops are determined for extended dikes, vertical cylinders, and edges of sills, and centers are for horizontal cylinders and spherical bodies). A depth calculation to the center of the source is more appropriate in this example because, as apparent from the derived η (between 2 and 3), from the observation location the source appears as a semi-compact object. The estimated depth of the object is accurate (0.56 m) with an error less than 0.1 m (less than 3% of the source-to-observation distance 2.17 m). We have attempted to test the stability of the result by adding various percentages

Table 2. The AN-EUL results from the airborne magnetic data over an I-beam section at the Badlands Bombing Range test site.

AAS_0 (nT/m)	AAS_1 (nT/m^2)	AAS_2 (nT/m^3)	η	z_o (m)
28.431	44.174	88.359	2.47	0.56*

*After subtracting the flight altitude (1.67 m).

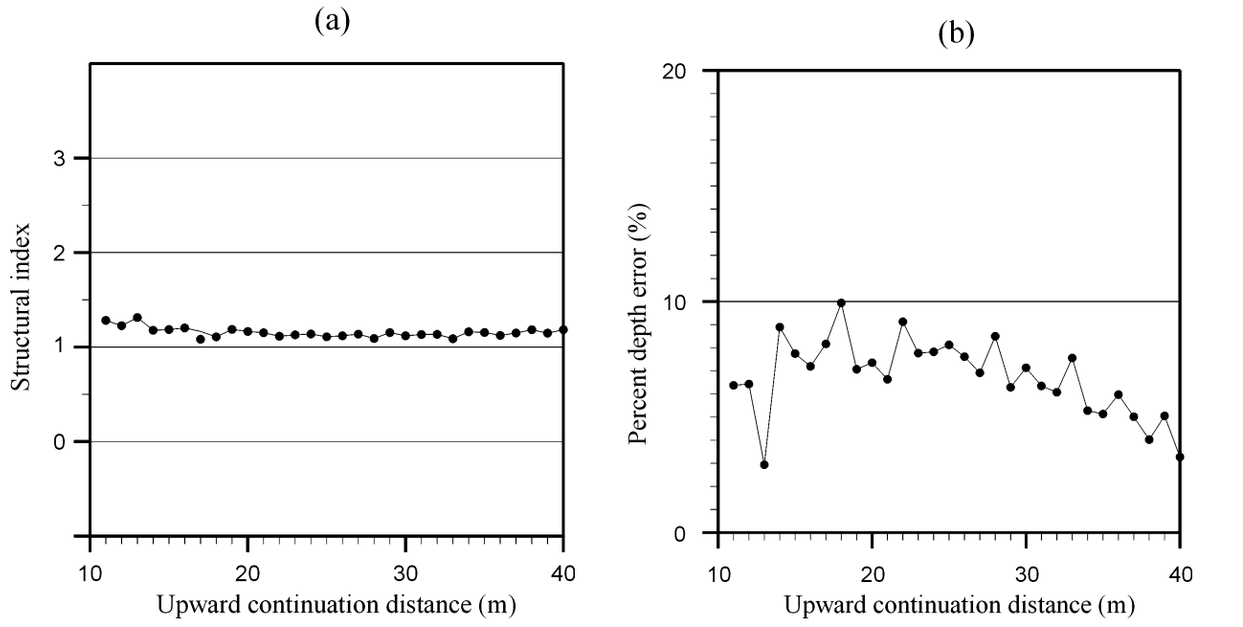

FIG. 5. Stability tests: (a) Estimate of the structural index (η) for the field data of the dike in southern Illinois (Figure 4a), (b) percent errors in the depth estimate for the field data of the dike in southern Illinois.

of pseudorandom noise (±1 nT) and computing the mean and standard deviation of the derived source-to-observation distances from 100 such tests. After upward continuing 0.1 m, the values for the source-to-observation distance have a mean of 2.19 m and standard deviation of 0.15 m. Since our method uses third-order derivatives, it is expected to be very sensitive to noise, yet the standard deviation of the noise tests is small compared to the source-to-observation distance and could be taken as a parameter that indicates stability of results.

Upward continuation of magnetic anomalies from 3D sources used in this paper to demonstrate their stability has been difficult for the following reasons. For 3D sources, *AAS* peaks do not overlie the epi-centroid for oblique inclinations (Salem et al., 2002), and errors caused by nonsuperposition of the peaks of AAS_0, AAS_1, and AAS_2 and the true epi-centroid location, even though appear to be negligible for the situations considered in this paper, are increased with upward continuation because the locations of the peaks and the epi-centroid diverge. Moreover, as shown by Ravat (1996a), the structural

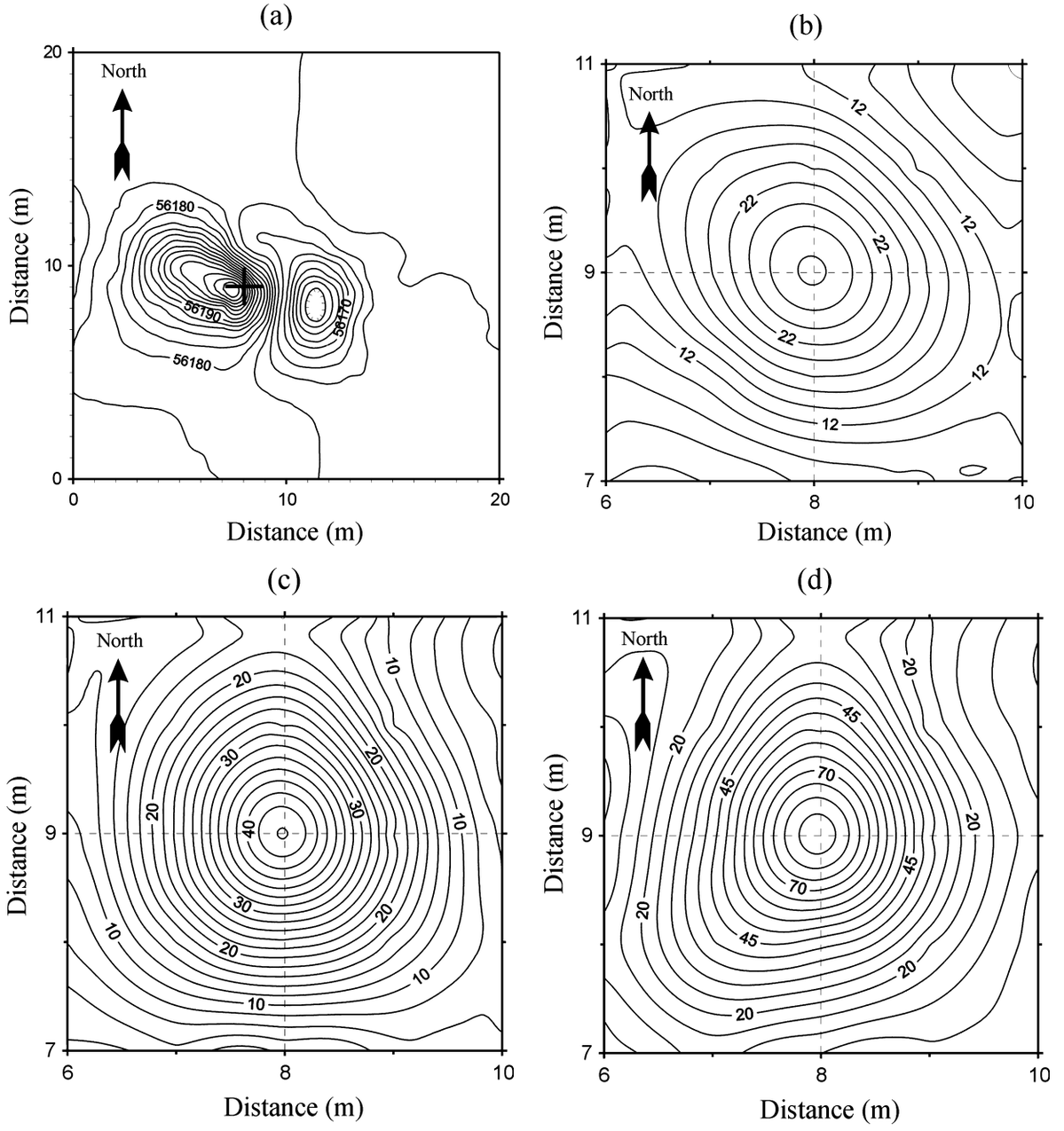

FIG. 6. (a) Isolated airborne magnetic anomaly over an I-beam section (cross showing its location) at the Badlands Bombing Range (BBR) test site (Gamey et al., 2000). Contour interval is 2 nT. (b) Analytic signal (AAS_0). Contour interval is 2 nT/m. (c) First-order derivative of the analytic signal (AAS_1). Contour interval is 2 nT/m^2. (d) Second-order derivative of the analytic signal (AAS_2). Contour interval is 5 nT/m^3.

index will change with increasing height, and the depth range and the magnetization parameters of the I-beam are such that the structural indices change rapidly by upward continuation of the original grid.

CONCLUSION

In this paper, we present a new method (AN-EUL) for automatic interpretation of magnetic data using a combination of the analytic signal and Euler methods. AN-EUL provides generalized equations to estimate both the depth and the geometry of magnetic sources at the location of a maximum in the amplitude of the analytic signal (*AAS*). The method uses the third derivative of magnetic anomaly and, therefore, is sensitive to noise in the data. In this study, it was tested using synthetic and field magnetic anomaly data and yielded results that agreed with the known source parameters. For well-isolated anomalies, the method may be automated because it does not require any assumptions about the nature of the source or its magnetization. It is amenable for application to both profile and grid magnetic data. Because the depth and structural index are derived from the successive derivatives of the total intensity anomaly, the method is less likely to be susceptible to inaccuracies in the isolation of the residual anomaly. However, as with all gradient interpretation methods, the resolution of this method is a function of the data quality and the observation spacing and, hence, the method requires high-resolution data.

ACKNOWLEDGMENTS

We greatly appreciate constructive and thoughtful comments of Dr. Richard Hansen, Dr. George Leblanc, and the Editor Dr. Joao Silva. We are also grateful to Dr. Alan Reid for his comments on this work. The authors would like to thank Oak Ridge National Laboratory for providing the airborne magnetic data and Kari Kirkham for providing the ground magnetic data. AS's work on this paper was made possible by funding from the Japan Society for the Promotion of Science (JSPS). DR's work on this paper was made possible by funding from NASA.

REFERENCES

Atchuta Rao, D., Ram Babu, H. V., and Sanker Narayan P. V., 1981, Interpretation of magnetic anomalies due to dikes: The complex gradient method: Geophysics, **46**, 1572–1578.

Bastani, M., and Pedersen, L. B., 2001, Automatic interpretation of magnetic dikes parameters using the analytic signal technique: Geophysics, **66**, 551–561.

Blakely, R. J., 1995, Potential theory in gravity and magnetic applications: Cambridge Univ. Press.

Debeglia, N., and Corpel, J., 1997, Automatic 3-D interpretation of potential field data using analytic signal derivatives: Geophysics, **62**, 87–96.

Gamey, T. J., Doll, W. E., and Bell, D. T., 2000, Airborne UXO detection technology demonstration: Proc. Symp. on the Application of Geophysics to Engineering and Environmental Problems (SAGEEP'2000), 57–66.

Hildenbrand, T. G., and Ravat, D., 1997, Geophysical setting of the Wabash Valley fault system: Seis. Res. Lett., **68**, 567–585.

Hsu, S. K., Sibuet, J. C., and Shyu, C. T., 1996, High-resolution detection of geologic boundaries from potential anomalies: An enhanced analytic signal technique: Geophysics, **61**, 373–386.

Hsu, S. K., Coppens, D., and Shyu, C. T., 1998, Depth to magnetic source using the generalized analytic signal: Geophysics, **63**, 1947–1957.

Kirkham, K., 2001, Investigations of a high-resolution aeromagnetic survey over the southeastern portion of the Illinois Basin: M.Sc. thesis, Southern Illinois University of Carbondale.

MacLeod, I. N., Jones, K., and Dai, T. F., 1993, 3-D Analytic signal in the interpretation of total magnetic field data at low magnetic latitudes: Expl. Geophys., **24**, 679–688.

Nabighian, M. N., 1972, The analytic signal of two-dimensional magnetic bodies with polygonal cross-section: Its properties and use for automated anomaly interpretation: Geophysics, **37**, 507–517.

———1974, Additional comments on the analytic signal of two-dimensional magnetic bodies with polygonal cross-section: Geophysics, **39**, 85–92.

———1984, Toward a three-dimensional automatic interpretation of potential-field data via generalized Hilbert transforms: Fundamental relations: Geophysics, **49**, 780–786.

Nelson, J. B., 1988, Comparison of gradient analysis techniques for two-dimensional magnetic sources: Geophysics, **53**, 1088–1095.

Pedersen, L. B., 1989, Relations between horizontal and vertical gradients of potential fields: Geophysics, **54**, 662, 663.

Ravat, D., 1996a, Analysis of the Euler method and its applicability in environmental magnetic investigations: J. Environmental. Eng. Geophys., **1**, 229–238.

———1996b, Magnetic properties of unrusted steel drums from laboratory and field-magnetic measurements: Geophysics, **61**, 1325–1335.

Reid, A. B., Allsop, J. M., Granser, H., Millet, A. J., and Somerton, I. W., 1990, Magnetic interpretation in three dimensions using Euler deconvolution: Geophysics, **55**, 80–91.

Roest, W. R., Verhoef, J., and Pilkington, M., 1992, Magnetic interpretation using 3-D analytic signal: Geophysics, **57**, 116–125.

Salem, A., Ravat, D., Gamey, T. J., and Ushijima, K., 2002, Analytic signal approach and its applicability in environmental magnetic investigations, J. Appl. Geophys., **49**, 231–244.

Smith, R. S., Thurston, J. B., Dai, T. F., and MacLeod, I. N., 1998, iSPI—the improved source parameters imaging method: Geophys. Prosp., **46**, 141–151.

Talwani, M., 1965, Computation with the help of a digital computer of magnetic anomalies caused by arbitrary shape: Geophysics, **30**, 797–817.

Thompson, D. T., 1982, "EULDPH" A new technique for making computer-assisted depth estimates from magnetic data: Geophysics, **47**, 31–37.

Thurston, J. B., and Smith, R. S., 1997, Automatic conversion of magnetic data to depth, dip, susceptibility contrast using the SPI method: Geophysics, **62**, 807–813.

Thurston, J., Guillon, J. C., and Smith, R., 1999, Model-independent depth estimation with the SPI method: 69th Ann. Internat. Mtg: Soc. of Expl. Geophys., Expanded Abstracts, 403–406.

Wasilewski, P. J., and Mayhew, M. A., 1992, The Moho as a magnetic boundary revisited: Geophys. Res. Lett., **19**, 2259–2262.